GHOST: Hallucination-Inducing Image Generation for Multimodal LLMs

Aryan Yazdan Parast[1][*], **Parsa Hosseini**[2][*], **Hesam Asadollahzadeh**[1], **Arshia Soltani Moakhar**[2],
Basim Azam[1], **Soheil Feizi**[2], **Naveed Akhtar**[1]
[1]The University of Melbourne   [2]University of Maryland

Abstract

Object hallucination in Multimodal Large Language Models (MLLMs) is a persistent failure mode that causes the model to perceive objects absent in the image. This weakness of MLLMs is currently studied using static benchmarks with fixed visual scenarios, which preempts the possibility of uncovering model-specific or unanticipated hallucination vulnerabilities. We introduce **GHOST** (**G**enerating **H**allucinations via **O**ptimizing **S**tealth **T**okens), a method designed to **stress-test** MLLMs by actively generating images that induce hallucination. GHOST is fully automatic and requires no human supervision or prior knowledge. It operates by optimizing in the image embedding space to mislead the model while keeping the target object absent, and then guiding a diffusion model conditioned on the embedding to generate natural-looking images. The resulting images remain visually natural and close to the original input, yet introduce subtle misleading cues that cause the model to hallucinate. We evaluate our method across a range of models, including reasoning models like GLM-4.1V-Thinking, and achieve a hallucination success rate exceeding 28%, compared to around 1% in prior data-driven discovery methods. We confirm that the generated images are both high-quality and object-free through quantitative metrics and human evaluation. Also, GHOST uncovers **transferable** vulnerabilities: images optimized for Qwen2.5-VL induce hallucinations in GPT-4o at a 66.5% rate. Finally, we show that fine-tuning on our images mitigates hallucination, positioning GHOST as both a diagnostic and corrective tool for building more reliable multimodal systems.

1 Introduction

Multimodal large language models (MLLMs) [Liu et al., 2024, 2023, Bai et al., 2025a, Team et al., 2025] have demonstrated impressive performance across a wide range of vision and language tasks, including image captioning, visual question answering, and multimodal reasoning. However, they suffer from a potentially critical failure mode: **object hallucination**, where the model incorrectly predicts the presence of an object that is not present in the image. Such errors raise concerns about the reliability of MLLMs in safety-sensitive applications and underscore the need for systematic methods to stress-test their visual robustness.

Existing evaluations of object hallucination in MLLMs typically rely on static benchmarks, fixed visual scenarios, and curated image sets [Li et al., 2023, Hu et al., 2023, Leng et al., 2024, Lovenia et al., 2023]. While useful, these approaches constrain analysis to a fixed set of visual scenarios and fail to expose model-specific vulnerabilities. Moreover, they lack a systematic way to assess which types of images trigger hallucinations, making it difficult to determine whether these errors are isolated or indicative of deeper, structural failure modes. Identifying such patterns is crucial not only for understanding model behavior but also for mitigating these failures.

---

[*]Equal Contribution. Correspondence to: `phoseini@umd.edu`

Prompt: Is there a knife in this picture?

GHOST 👻

:GPT-4o   :Qwen2.5VL   :LLava1.6

:GLM4.1Thinking   :LLaMA3.2

No, there is no knife in the image. The image shows a banana on a decorative plate with floral patterns.

No, there is no knife in the image. The image shows a banana placed on a decorative plate.

No, there is no knife visible in the image. The image shows a banana on a plate.

No, there is no knife in the image. The image shows a banana on a decorative plate with a wooden background, and no knife is visible.

No, there is no knife in the image. Instead, a banana is placed on a plate with a floral pattern.

Yes, there is a knife in the image. A knife is visible behind the banana on the plate.

Yes, there is a knife in the image. It is placed on the plate next to the banana.

Yes, there is a knife in the image. It is resting on the plate alongside the banana.

Yes, there is a knife in the image. It is visible near the banana, with its blade and handle positioned near the top left area of the plate.

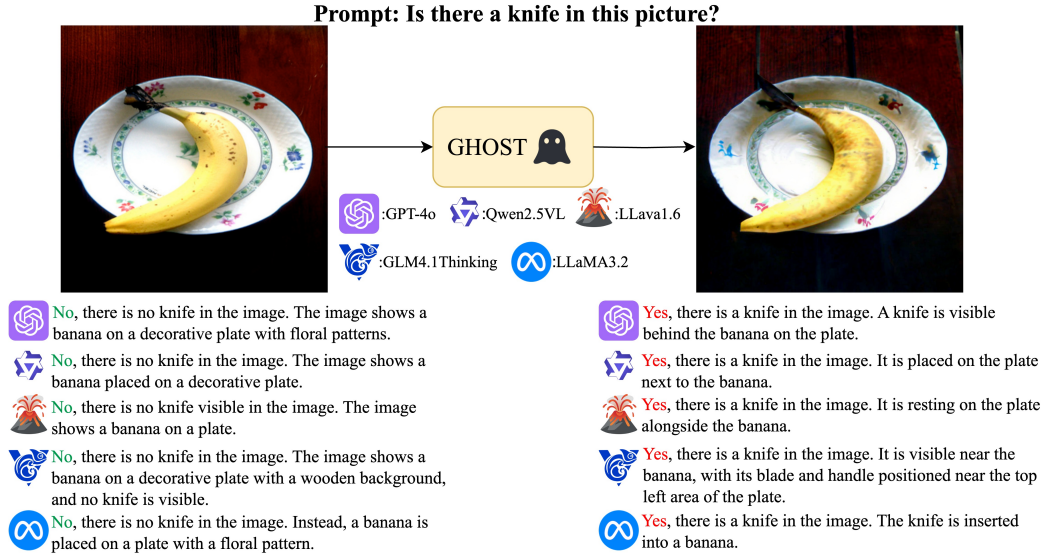Yes, there is a knife in the image. The knife is inserted into a banana.

Figure 1: (**Left**) All models correctly answer "No" when asked if there is a knife in the image. (**Right**) GHOST introduces subtle cues, and all models now hallucinate the presence of a knife.

To address these limitations, we introduce GHOST (Generating Hallucinations via Optimizing Stealth Tokens), a method designed to stress-test MLLMs by synthesizing hallucination-inducing images. Given an input image and a target object, GHOST generates a visually similar image that preserves the absence of the object but causes the model to incorrectly detect it. The edits introduced by GHOST are subtle and semantic, contextual cues that are perceptible to humans but do not introduce the object itself. This is accomplished by optimizing the image's CLIP embedding to elicit hallucination while regularizing against object insertion, then using it to guide the diffusion model to generate a natural-looking image.

Consider the example in Figure 1. The original image (left) shows a banana on a plate with no knife present, and multiple MLLMs correctly answer "No" when asked whether a knife is in the picture. However, after GHOST introduces subtle changes, such as modifying the banana's stem to resemble the edge of a knife, the models flip their answer to "Yes," hallucinating a knife. These misleading cues are not convincing to human observers, yet they are sufficient to push the models across the decision boundary.

One key innovation in GHOST is its design that decouples the optimization process from the image generator. Prior work on systematic failure image generation either omits feedback from the target model, limiting their ability to capture model-specific blind spots [Zhang et al., 2024, Wu et al., 2024], or uses resource-intensive and slow pipelines [Augustin et al., 2025]. In contrast, GHOST introduces a mapper that aligns the visual spaces of the target model and the diffusion model, enabling efficient optimization while preserving compatibility across different image generators and vision-language models.

Together, these components make GHOST scalable and effective: for instance, on Qwen2.5-VL [Bai et al., 2025a], GHOST generates 2,816 hallucination-inducing images out of 9,423 initial inputs, a 29% success rate–compared to 0.1% in DASH [Augustin et al., 2025]. GHOST also generalizes to reasoning-based MLLMs like GLM-4.1V-Thinking [Team et al., 2025], where it shifts the model's reasoning trajectory to justify the presence of a nonexistent object (Figure 7). The resulting images are natural and high quality, as demonstrated by the FID results in Table 2. Figure 2 shows qualitative examples, where each column compares an original image (top) with its GHOST-edited counterpart (bottom). The subtle semantic changes introduced by GHOST cause the model to hallucinate its presence. Human evaluation confirms that GHOST images remain object-free from a human perspective, with 89% of responses agreeing the target object is absent.

GHOST also reveals transferable vulnerabilities: images optimized for one model often cause hallucinations in others. For example, images generated for Qwen2.5-VL induce hallucinations in
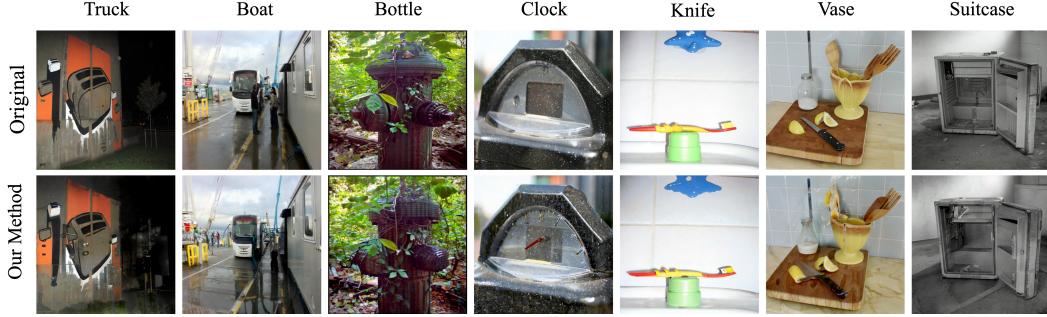
	Truck	Boat	Bottle	Clock	Knife	Vase	Suitcase
Original							
Our Method							

Figure 2: (**Top**) Input images, the MLLM does not hallucinate the target object. (**Bottom**) GHOST images, the MLLM hallucinates the object, despite its absence being clear to a human observer.

GPT-4o at a 66.5% rate (Table 3). GHOST thus exposes not just model-specific blind spots, but systemic vulnerabilities across MLLMs.

Finally, we demonstrate that GHOST can also aid in mitigation: fine-tuning on GHOST synthetic images improves model robustness on downstream hallucination benchmarks (Section 6.2), highlighting GHOST's potential as both a diagnostic and corrective tool.

2 Related works

Systematic Failures in MLLMs. Recent works have introduced frameworks to automatically identify failures in MLLMs [Tong et al., 2024a,b, Hosseini et al., 2025]. Tong et al. [2024b] highlight MLLMs' struggles with basic visual understanding, attributing them to limitations in CLIP-based vision encoders. In contrast, Tong et al. [2024a] focuses on failures stemming from the language modality. Hosseini et al. [2025] show that MLLMs often over-rely on spurious visual cues, leading to hallucinations when such cues are present but the object itself is absent. A large body of work has specifically examined object hallucination [Li et al., 2023, Leng et al., 2024, Lovenia et al., 2023, Hu et al., 2023, Wang et al., 2023], typically proposing benchmarks and evaluation protocols to quantify the issue. However, these approaches rely on curated image sets, constraining analysis to a fixed set of visual scenarios. In contrast, our method actively generates failure images, uncovering novel and unanticipated visuals that are unlikely to appear in static datasets.

Discovering Hallucinations through Image Generation. Some prior studies [Wu et al., 2024, Zhang et al., 2024] evaluate MLLMs on synthesized images generated via carefully designed prompts using text-to-image models. While these methods can reveal general failure modes, they do not incorporate feedback from the MLLM itself, limiting their ability to uncover model-specific vulnerabilities or adapt flexibly across models. In contrast, GHOST leverages model feedback and performs targeted optimization in the CLIP image space.

DASH [Augustin et al., 2025] is the most comparable prior work, as it also incorporates MLLM feedback for image generation. However, it operates directly over diffusion latents and requires the MLLM, the diffusion model, the generated image, and an object detector to all remain in the optimization loop, making it both time and resource intensive and forcing the use of a distilled single-step diffusion model. Moreover, DASH ultimately retrieves similar images from the real dataset based on the generated ones. GHOST addresses these limitations with a decoupled and more efficient design. In Section 5 and Appendix B, we provide comparisons with DASH.

Robustness of Diffusion Representations. It is well-established that deep networks trained with empirical risk minimization (ERM) often rely on spurious correlations to make predictions [Sagawa et al., 2019, Kirichenko et al., 2022, Noohdani et al., 2024, Parast et al., 2025]. Recent studies have also identified such correlations in CLIP [Radford et al., 2021b] and autoregressive vision-language models [Wang et al., 2024a, Varma et al., 2024, Kim et al., 2023, Ye et al., 2024, Zheng et al., 2024]. In contrast, diffusion models have shown greater robustness in their learned representations, as they aim to approximate the underlying data distribution rather than optimizing for a specific downstream task [Li et al., 2024, Luo et al., 2024]. Li et al. [2024] demonstrate that U-Net-based latent diffusion models [Rombach et al., 2022] are less prone to shortcut solutions compared to discriminative models.

DEEM [Luo et al., 2024] further argues that vision encoders in MLLMs, often based solely on models like CLIP-ViT, can be improved using the generative feedback of diffusion models to align the semantic distributions of the image encoder. They showed this alignment enhances robustness to out-of-distribution inputs and reduces visual hallucinations. Motivated by these insights, we leverage diffusion models to probe vulnerabilities in MLLMs.

Adversarial Attacks on MLLMs. GHOST can be viewed as a form of adversarial generation, but we highlight key distinctions from prior work. Methods like AnyAttack [Zhang et al., 2025a] and AttackVLM [Zhao et al., 2023] operate in pixel space and preserve the overall image semantics, aiming for imperceptible perturbations. In contrast, GHOST inserts semantic-level misleading cues, plausible to humans yet triggering hallucinations in MLLMs. While adversarial examples are sometimes transferable across models, GHOST exhibits a different kind of transfer: cues crafted for one model generalize to others, pointing to shared failure modes and spurious biases. Our approach is closer in spirit to content-based adversarial attacks such as Chen et al. [2023], but differs in both setting (image classifiers vs. MLLMs) and objective (causing hallucination rather than misclassification).

3 Problem Setup

We consider an MLLM $\mathcal{M}$ that integrates a vision encoder $\mathcal{V}_{\mathcal{M}}$ with a language model backbone $f_{\mathcal{M}}$. The text input is denoted as $\mathbf{X}_q \in \mathcal{L}$, where $\mathcal{L}$ is the space of language, and the image input as $\mathbf{X}_v \in \mathcal{I}$, where $\mathcal{I}$ is the space of images. The vision encoder $\mathcal{V}_{\mathcal{M}} : \mathcal{I} \rightarrow \mathbb{R}^{N \times d_{\mathcal{M}}}$ maps the image $\mathbf{X}_v$ into a sequence of N vision tokens of dimension $d_{\mathcal{M}}$, denoted by $\mathbf{Z}_v = \mathcal{V}_{\mathcal{M}}(\mathbf{X}_v)$. These tokens, together with the text input $\mathbf{X}_q$, are passed to the LLM backbone $f_{\mathcal{M}}$, which generates an output sequence $Y = (y_1, \ldots, y_T)$ autoregressively. Each token y_t is sampled from the conditional probability $p(y_t \mid y_{<t}, \mathbf{X}_q, \mathbf{Z}_v) = f_{\mathcal{M}}(y_{<t}, \mathbf{X}_q, \mathbf{Z}_v)$.

We also consider a Latent Diffusion Model $\mathcal{G}$, which generates an image $\tilde{\mathbf{X}}_v = \mathcal{G}(\mathbf{X}_v \mid c)$ given an initial image $\mathbf{X}_v$ and a conditioning signal c. We employ Stable Diffusion unCLIP [Rombach et al., 2022], where c is an embedding in the CLIP embedding space. Formally, let $\mathcal{V}_{\text{CLIP}} : \mathcal{I} \cup \mathcal{L} \rightarrow \mathbb{R}^{d_{\text{CLIP}}}$ denote the CLIP encoder that learned joint representation for text and images. Note that $\mathcal{M}$ and $\mathcal{G}$ use different vision encoders; therefore, we introduce a mapper $\Pi : \mathbb{R}^{d_{\text{CLIP}}} \rightarrow \mathbb{R}^{N \times d_{\mathcal{M}}}$ to bridge these embedding spaces. Given an initial image $\mathbf{X}_v$ without the target object t, a prompt $\mathbf{X}_q$ of the form "Do you see a t in the image?", and a target token y^* (e.g.,"Yes"), we aim to find an embedding $c \in \mathbb{R}^{d_{\text{CLIP}}}$ that satisfies the following constraints:

1. **Proximity to the original image:** c remains close to the initial embedding $c_0 = \mathcal{V}_{\text{CLIP}}(\mathbf{X}_v)$
2. **Absence of the target object semantics:** c doesn't encode the target object itself.
3. **Inducing hallucination:** $\mathcal{M}$ assigns high probability to answering the target token y^*

$$p(y^* \mid \mathbf{X}_q, \Pi(c)) \geq \tau_{\text{yes}} \qquad (1)$$

where τ_{yes} is a confidence threshold.

We condition the diffusion model on the optimized embedding c to generate an image $\tilde{\mathbf{X}}_v = \mathcal{G}(\mathbf{X}_v \mid c)$ and check whether $\mathcal{M}$ hallucinates the target object. Diffusion unCLIP enables this process by allowing the image generation to be conditioned on a CLIP image embedding. Full pipeline and implementation details are provided in Section 4.

4 Method

This section introduces GHOST (**G**enerating **H**allucinations via **O**ptimizing **S**tealth **T**okens), a fully automated pipeline for stress-testing object hallucinations in MLLMs. We begin with the implementation of the mapper Π, then describe our optimization procedure, and finally explain how the diffusion model generates images within the pipeline.

4.1 Bridging Embedding Spaces

To incorporate feedback from the MLLM into the generation process, a naive approach would require backpropagating through the entire pipeline – including the MLLM, the generated image, and the
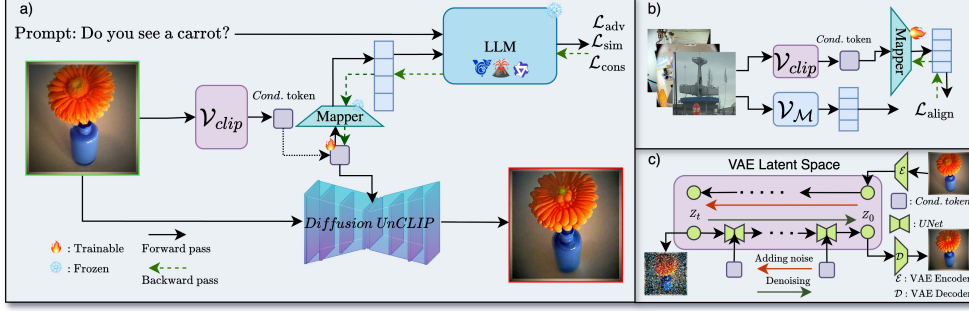
Figure 3: a) Overview of GHOST. We optimize only the CLIP embedding, then condition unCLIP on it, see (c) for decoding details. b) Training setup for the MLP, which aligns CLIP embeddings with the MLLM vision encoder using an MSE loss. c) A partially noised latent of the original image is denoised conditioned on the optimized embedding.

diffusion model– which is computationally expensive. To overcome this, we introduce a mapper (Π) that bridges the embedding spaces of the MLLM and the diffusion model, enabling more efficient optimization. We implement Π as an MLP and find that this simple design is sufficient for our purposes. Given an MLLM $\mathcal{M}$ and a dataset $\mathcal{D}$ of images, the MLP is trained with a mean squared error (MSE) objective:

$$\mathcal{L}_{\text{align}} = ||\Pi(\mathcal{V}_{\text{CLIP}}(\mathbf{X}v)) - \mathcal{V}_{\mathcal{M}}(\mathbf{X}_v)||_2^2, \tag{2}$$

where $\mathbf{X}_v \in \mathcal{D}$. The training setup is illustrated in Figure 3b. For more details see Appendix C.

4.2 Optimization Objective

With the mapper Π trained, we now introduce the attack. Given a target object t and an initial image $\mathbf{X}_v$ that do not contain t, we optimize the CLIP embedding $z = \mathcal{V}_{\text{CLIP}}(\mathbf{X}_v)$ so that it tends to satisfy the conditions from Section 3.

Proximity to the original image: We regularize c to remain close to the embedding of the initial real image. This prevents excessive drift and preserves high-level semantics. Formally, let c_0 be the CLIP embedding of the original image, we impose an ℓ_2 penalty:

$$\mathcal{L}_{reg} = \left\| c - c_0 \right\|_2^2 \tag{3}$$

Absence of the target object semantics: To discourage c from encoding the target object directly, we penalize its similarity to the CLIP embedding of the object's textual descriptions. Rather than relying on a single prompt, we define a set of textual templates $\mathcal{T}_{clip}$ (e.g., "a photo of a t") to represent the target object (See Appendix E.2 for more details). We compute the expected cosine similarity between c and the CLIP embeddings of these templates:

$$\mathcal{L}_{\text{clip}} = \mathbb{E}_{\mathbf{T}_q \sim \mathcal{T}_{\text{clip}}} \left[\cos(c, \mathcal{V}_{\text{CLIP}}(\mathbf{T}_q)) \right] \tag{4}$$

Inducing hallucination: To mislead the model to perceive the target object, we see the probability that the LLM assigns to the target token y^*. Specifically, given a query prompt $\mathbf{X}_q$ of the form "Do you see a t in the image?", we define the loss as:

$$\mathcal{L}_{\text{adv}} = -\log p(y^\star \mid \mathbf{X}_q, \Pi(c)) \tag{5}$$

To prevent overfitting to a single phrasing, we construct a diverse set of semantically equivalent query templates and randomly sample $\mathbf{X}_q$ from this set at each optimization step (The templates are provided in AppendixE.4).

Our joint objective combines all components:

$$\mathcal{L}_{\text{total}} = \mathcal{L}_{\text{adv}} + \lambda_{clip} \mathcal{L}_{\text{clip}} + \lambda_{reg} \mathcal{L}_{\text{reg}}, \tag{6}$$
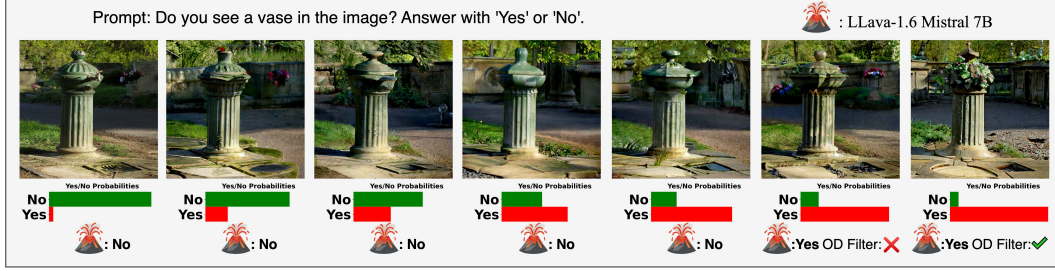
5

Figure 4: Optimization steps toward hallucination. We show the model's Yes/No probabilities for the optimized embedding at each step. Images are then generated by conditioning diffusion on that embedding. As "Yes" confidence increases, misleading cues (e.g., vase-like structures) emerge. Samples flagged by OWLv2 are discarded.

where λ_{clip}, λ_{reg} are hyperparameters that control the relative importance of these terms. We minimize this loss using the AdamW [Loshchilov and Hutter, 2017] optimizer. An overview of this pipeline is illustrated in Figure 3a, and ablation studies are provided in Section 6.

After each optimization step, we check whether the model's probability for the target token exceeds the threshold confidence τ_{yes}. We perform at most M optimization steps per image. If the probability does not surpass τ_{yes} within M steps, we discard the result and move to the next image. Otherwise, once the threshold is met, we use the current embedding z to generate a candidate image via the diffusion model, described in the next section.

4.3 Guided Diffusion

As shown in Figure 3c, instead of starting from pure noise, we begin the reverse process from a partially noised latent of the original image. This design encourages the final image to preserve the high-level structure of the input while still allowing for subtle semantic shifts that can induce hallucination. Concretely, we encode the original image $\mathbf{X}_v$ into its VAE latent representation, apply forward diffusion for t steps to obtain z_t, and then condition the reverse denoising on c. The noise level t controls the trade-off between preserving the original image structure and allowing space for misleading cues. To account for diffusion stochasticity, we allow up to $N = 4$ generation attempts per image. More details are provided in Appendix D.

We use an open-vocabulary object detector, OWLv2 [Minderer et al., 2024], as a filtering step to verify that the generated image does not actually contain the target object. If OWLv2 detects the target object, we conservatively discard the sample. Only when the model hallucinates the object and OWLv2 confirms its absence do we consider the hallucination-inducing process successful. Figure 4 provides a qualitative example: as we optimize the CLIP embedding to increase the model's confidence in answering "Yes," the images gradually incorporate misleading visual features, in this case, vase-like structures. Note that this figure is illustrative only; we do not generate images at each step of optimization.

5 Experiments

In this section, we present both quantitative and qualitative results of GHOST on three open-source MLLMs. We also evaluate the transferability of GHOST-generated images across a diverse set of additional models.

5.1 Results

Models. We evaluate GHOST on three open-source MLLMs accessed via HuggingFace: Qwen2.5-VL-7B-Instruct [Bai et al., 2025a], LLaVA-v1.6-Mistral-7B [Liu et al., 2024], and GLM-4.1V-Thinking [Team et al., 2025].

Dataset. We select 10 target object classes from the COCO dataset [Lin et al., 2014]. For each class, we begin by excluding all images containing the target object based on COCO annotations. Among the remaining negatives, we select the top 1,000 images with the highest CLIP similarity to the object

Table 1: **GHOST and DASH [Augustin et al., 2025] results on COCO.** "Samples" reflects the size of the input pool each method operates over.

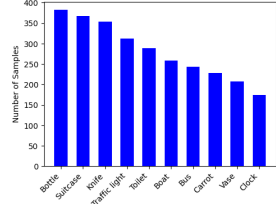| Method	Model	Samples	Hallucination	Success
GHOST	Qwen2.5-VL	9423	2816	29.9%
	LLaVA-v1.6	8786	2468	28.1%
	GLM-4.1V	8889	2880	32.4%
DASH-LLM	Qwen2.5-VL	118,000	57	0.1%
	LLaVA-v1.6	118,000	153	0.1%
DASH-OPT	Qwen2.5-VL	118,000	42	0.1%

Figure 5: Class-wise hallucination samples generated by GHOST across 10 objects for Qwen.

name. This sorting identifies visually diverse yet semantically related contexts where hallucination is more likely to occur. In Appendix E.1, we also evaluate GHOST without CLIP sorting and show that our results remain consistent. To isolate GHOST-induced failures, we discard any image where the MLLM already predicts the target object before optimization.

Results. We present the GHOST results in Table 1. For each model, "Samples" refers to the number of images (out of the initial 10,000 COCO images) in which the model does not perceive the target object. We then report how many hallucination-inducing images GHOST successfully generates, followed by the success rate (i.e., number of hallucinations divided by the number of samples). We also include results from DASH [Augustin et al., 2025], applied to the COCO dataset. Despite operating on a much smaller image pool, GHOST discovers orders of magnitude more hallucination-inducing samples. For instance, GHOST identifies 2,816 successful cases for Qwen2.5-VL, while DASH-LLM and DASH-OPT combined find only 99. It is important to note that DASH was originally designed to search over ReLAION-5B [LAION, 2024], a massive web-scale dataset. Its goal is not to maximize hallucination count, but to uncover naturally occurring failure cases across large-scale image corpora. Our comparison on COCO is intended to provide a point of reference against an existing method that shares a similar objective: identifying systematic hallucination-inducing inputs. Further details about our DASH experiments are provided in Appendix B.

We also break down GHOST's performance by object class in Figure 5. GHOST discovers a substantial number of hallucination cases for all classes. More details on the class-wise results of our method are provided in Appendix F.

Image Quality. To evaluate the quality of the samples generated by GHOST, we conduct both qualitative and quantitative analyses. Figure 6 presents visual comparisons between GHOST and two baseline diffusion methods: Stable Diffusion v2.1 [Rombach et al., 2022], where we prompt the model using the COCO caption of the image, and Stable Diffusion unCLIP, where the diffusion is conditioned on the CLIP embedding of the image. GHOST preserves the semantics of the original image while introducing minimal visual artifacts. Table 2 reports Fréchet Inception Distance, FID scores [Heusel et al., 2017], evaluating each method along two axes: (i) realism, measured by FID against COCO validation images, and (ii) semantic fidelity, measured by FID against the initial images used in diffusion. While GHOST achieves comparable realism to baseline methods, it outperforms them in semantic preservation, confirming its advantage in maintaining visual identity. We observe higher FID scores for GLM hallucinations, likely due to the model's reasoning nature. Since we optimize a "thinking" token rather than the final answer directly, the optimization path is less aligned with the hallucination objective, making it harder to induce consistent visual drift. Also more qualitative samples are provided in Appendix F.

Reasoning Model. We evaluate GHOST on GLM-4.1V-Thinking [Team et al., 2025], a multimodal model trained with a reasoning-centric framework. The model structures its responses in two stages: it first generates a reasoning trace enclosed within `<think>...</think>` tokens, followed by a final answer within `<answer>...</answer>`. To adapt GHOST to this format, we use the probability of the token `"Yes"` at the first decoding step after the `<think>` token. This allows us to keep the optimization objective and runtime consistent with other models. We find that, despite not explicitly optimizing for the final answer, this is sufficient to induce hallucinated `"Yes"` responses in the final
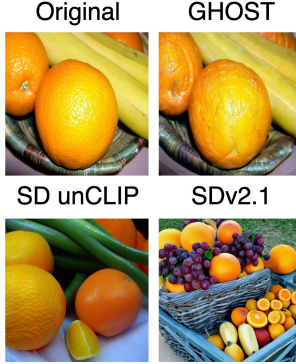
Figure 6: Qualitative comparison of generated images.

Table 2: FID scores (lower is better) for different diffusion methods. Each method is evaluated for realism (vs. COCO validation images) and semantic preservation (vs. the initial images used in diffusion).

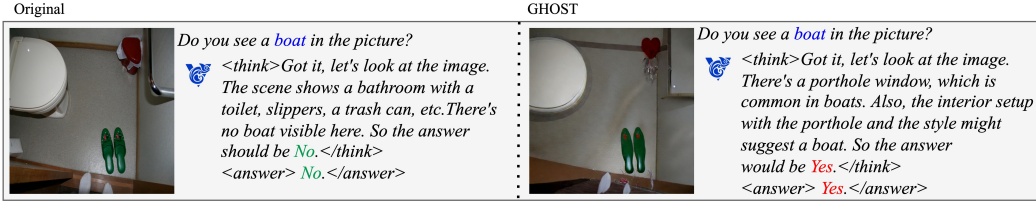| Method	Qwen2.5-VL	LLaVA-v1.6	GLM4.1V
Distributional Realism			
SD v2.1	**46.19**	**48.42**	44.79
SD unCLIP	46.51	50.20	**44.76**
GHOST	47.03	50.78	51.70
Semantic Fidelity			
SD v2.1	41.71	42.64	39.85
SD unCLIP	31.67	35.47	**32.07**
GHOST	**25.00**	**26.39**	34.94

Figure 7: Applying GHOST to a reasoning model (GLM-4.1V-Thinking).

output. A qualitative example is shown in Figure 7, where GHOST edits shift the model's reasoning trajectory to justify the presence of a nonexistent object.

Human Evaluation. To evaluate whether GHOST images preserve the absence of the target object from a human perspective, we asked 40 peers to review the images, resulting in over 3,000 total votes. They were shown the final GHOST images and asked whether they could see the target object. On average, 89% of responses for images optimized w.r.t LLaVA-v1.6 and 86.3% for Qwen2.5-VL indicated that the object was not present. For reference, DASH [Augustin et al., 2025] reports that 5.2% of their images contained the object and 7.8% were ambiguous, implying that 87% of their samples were perceived as object-free. Additional details are provided in Appendix A.

5.2 Transferability

We evaluate how images generated by GHOST on one model transfer to others. In addition to the three source models, we include two larger open-source models: LLaMA3.2 11B [Meta, 2024] and Aya 32B [Dash et al., 2025], as well as two closed-source models: GPT-4o [OpenAI, 2024] and Gemini2.5-Flash [Comanici et al., 2025]. As shown in Table 3, images optimized on Qwen2.5-VL achieve a 66.5% hallucination success rate on GPT-4o. These results suggest that different models share common failure patterns. More details are provided in Appendix F.

6 Ablation Studies

6.1 Effect of Hyperparameters

Effect of τ. We study how the confidence threshold τ impacts GHOST's success by varying $\tau \in \{0.5, 0.6, 0.7, 0.8, 0.9\}$ on 400 images from two objects (200 images each), while keeping the number of optimization steps fixed at 100 and using the same learning rate. A higher τ requires the optimized embedding to achieve higher $p(y^* \mid \mathbf{X}_q, \Pi(c))$, making optimization harder. As expected, this reduces the number of images that meet the threshold within the allowed steps (see Appendix E.7). However, as shown in Figure 9, images generated from embeddings optimized with higher τ are more likely to induce hallucination. These results confirm that the confidence score $p(y^* \mid \mathbf{X}_q, \Pi(c))$

Table 3: Transferability of hallucinations across models. Each row corresponds to the model used, and each column shows the success rate (%) on a target model.

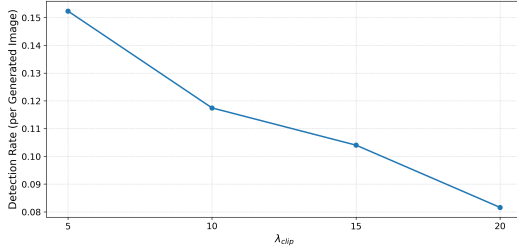| Model	Qwen2.5-VL	LLaVA-v1.6	GLM4.1V	GPT-4o	Aya	LLaMA3.2	Gemini
Qwen2.5-VL	–	62.2	72.0	66.5	71.1	65.8	58.6
LLaVA-v1.6	52.6	–	50.5	50.5	54.4	49.7	42.8
GLM4.1V	63.2	57.1	–	63.8	67.6	69.1	53.8

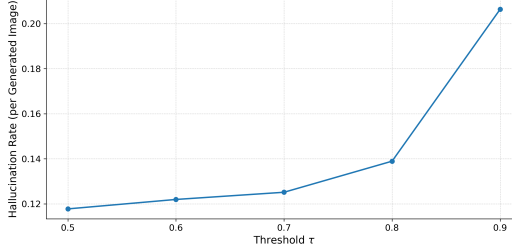Figure 8: Larger λ_{clip} leads to less objects.

Figure 9: Larger τ leads to more hallucination.

serves as a meaningful proxy for the model's belief in object presence, even though the optimization is decoupled from the diffusion process.

Effect of λ_{clip}. We evaluate the impact of λ_{clip} using the same setup. As shown in Figure 8, increasing λ_{clip} reduces the object detection rate per generated image. This confirms that stronger penalties on CLIP similarity discourage the diffusion model from generating images containing the object. Additional results are provided in Appendix E.6.

Effect of λ_{reg}. As shown in Appendix E.5, increasing $\lambda_{reg} \in \{1.0, 1.5, 2.0\}$ on GLM samples lowers FID scores, indicating that this term helps preserve visual realism.

6.2 Mitigation

As a small toy setup, we fine-tune Qwen2.5-VL using GHOST images. Following DASH [Augustin et al., 2025], we include both positive and negative samples to avoid forgetting of object concepts. However, unlike DASH, which uses real COCO images as positives, we generate both positives and negatives synthetically using Diffusion unCLIP to ensure consistency in visual style. This prevents the model from simply learning to reject all synthetic content.

Table 4 shows that fine-tuning improves robustness to hallucination-inducing images generated by other models (LLaVA and GLM), despite never seeing them during training. We also observe improvements on the POPE [Li et al., 2023] benchmark, while DASH reports no gains on POPE. Finally, performance on general tasks such as VQAv2 and COCO captioning remains nearly unchanged, suggesting that fine-tuning likely preserves general capabilities.

Table 4: Fine-tuning Qwen2.5-VL on GHOST images improves robustness to hallucination.

	GHOST-LLaVA	GHOST-GLM	POPE	VQAv2	Caption
Baseline	52.6	63.1	88.5	**73.5**	**89.5**
Finetuned	**7.0**	**7.3**	**90.7**	73.4	89.4

7 Conclusion

We introduce GHOST, a pipeline for generating images that induce hallucinations in MLLMs by inserting minimal cues. Our method leverages diffusion models to craft these cues, demonstrating that their vision space aligns well with the visual representations used by MLLMs. Beyond a single model, GHOST reveals cross-modal failure modes that are not detectable by prior works. We hope GHOST can help and inspire future work toward building more robust and reliable multimodal systems.

Acknowledgments

References

Maximilian Augustin, Yannic Neuhaus, and Matthias Hein. Dash: Detection and assessment of systematic hallucinations of vlms. In *ICCV*, 2025.

Mohammad Azizmalayeri, Arshia Soltani Moakhar, Arman Zarei, Reihaneh Zohrabi, Mohammad Manzuri, and Mohammad Hossein Rohban. Your out-of-distribution detection method is not robust! *Advances in Neural Information Processing Systems*, 35:4887–4901, 2022.

Shuai Bai, Keqin Chen, Xuejing Liu, Jialin Wang, Wenbin Ge, Sibo Song, Kai Dang, Peng Wang, Shijie Wang, Jun Tang, Humen Zhong, Yuanzhi Zhu, Mingkun Yang, Zhaohai Li, Jianqiang Wan, Pengfei Wang, Wei Ding, Zheren Fu, Yiheng Xu, Jiabo Ye, Xi Zhang, Tianbao Xie, Zesen Cheng, Hang Zhang, Zhibo Yang, Haiyang Xu, and Junyang Lin. Qwen2.5-vl technical report. *arXiv preprint arXiv:2502.13923*, 2025a.

Tianyi Bai, Yuxuan Fan, Jiantao Qiu, Fupeng Sun, Jiayi Song, Junlin Han, Zichen Liu, Conghui He, Wentao Zhang, and Binhang Yuan. Hallucination at a glance: Controlled visual edits and fine-grained multimodal learning. *arXiv preprint arXiv:2506.07227*, 2025b.

Zhaoyu Chen, Bo Li, Shuang Wu, Kaixun Jiang, Shouhong Ding, and Wenqiang Zhang. Content-based unrestricted adversarial attack. *Advances in Neural Information Processing Systems*, 36:51719–51733, 2023.

Gheorghe Comanici, Eric Bieber, Mike Schaekermann, Ice Pasupat, Noveen Sachdeva, Inderjit Dhillon, Marcel Blistein, Ori Ram, Dan Zhang, Evan Rosen, et al. Gemini 2.5: Pushing the frontier with advanced reasoning, multimodality, long context, and next generation agentic capabilities. *arXiv preprint arXiv:2507.06261*, 2025.

Saurabh Dash, Yiyang Nan, John Dang, Arash Ahmadian, Shivalika Singh, Madeline Smith, Bharat Venkitesh, Vlad Shmyhlo, Viraat Aryabumi, Walter Beller-Morales, et al. Aya vision: Advancing the frontier of multilingual multimodality. *arXiv preprint arXiv:2505.08751*, 2025.

Martin Heusel, Hubert Ramsauer, Thomas Unterthiner, Bernhard Nessler, and Sepp Hochreiter. Gans trained by a two time-scale update rule converge to a local nash equilibrium. *Advances in neural information processing systems*, 30, 2017.

Jonathan Ho, Ajay Jain, and Pieter Abbeel. Denoising diffusion probabilistic models, 2020. URL `https://arxiv.org/abs/2006.11239`.

Parsa Hosseini, Sumit Nawathe, Mazda Moayeri, Sriram Balasubramanian, and Soheil Feizi. Seeing what's not there: Spurious correlation in multimodal llms. *arXiv preprint arXiv:2503.08884*, 2025.

Edward J Hu, yelong shen, Phillip Wallis, Zeyuan Allen-Zhu, Yuanzhi Li, Shean Wang, Lu Wang, and Weizhu Chen. LoRA: Low-rank adaptation of large language models. In *International Conference on Learning Representations*, 2022. URL `https://openreview.net/forum?id=nZeVKeeFYf9`.

Hongyu Hu, Jiyuan Zhang, Minyi Zhao, and Zhenbang Sun. Ciem: Contrastive instruction evaluation method for better instruction tuning. *arXiv preprint arXiv:2309.02301*, 2023.

Jae Myung Kim, A Koepke, Cordelia Schmid, and Zeynep Akata. Exposing and mitigating spurious correlations for cross-modal retrieval. In *Proceedings of the IEEE/CVF Conference on Computer Vision and Pattern Recognition*, pages 2585–2595, 2023.

Polina Kirichenko, Pavel Izmailov, and Andrew Gordon Wilson. Last layer re-training is sufficient for robustness to spurious correlations. *arXiv preprint arXiv:2204.02937*, 2022.

LAION. Releasing re-laion-5b: transparent iteration on laion-5b with additional safety fixes. `https://laion.ai/blog/relaion-5b/`, 2024. Accessed: 30 aug, 2024.

Sicong Leng, Yun Xing, Zesen Cheng, Yang Zhou, Hang Zhang, Xin Li, Deli Zhao, Shijian Lu, Chunyan Miao, and Lidong Bing. The curse of multi-modalities: Evaluating hallucinations of large multimodal models across language, visual, and audio. *arXiv preprint arXiv:2410.12787*, 2024.

Alexander Cong Li, Ananya Kumar, and Deepak Pathak. Generative classifiers avoid shortcut solutions. In *The Thirteenth International Conference on Learning Representations*, 2024.

Yifan Li, Yifan Du, Kun Zhou, Jinpeng Wang, Wayne Xin Zhao, and Ji-Rong Wen. Evaluating object hallucination in large vision-language models. *arXiv preprint arXiv:2305.10355*, 2023.

Tsung-Yi Lin, Michael Maire, Serge J. Belongie, James Hays, Pietro Perona, Deva Ramanan, Piotr Dollár, and C. Lawrence Zitnick. Microsoft COCO: common objects in context. In David J. Fleet, Tomás Pajdla, Bernt Schiele, and Tinne Tuytelaars, editors, *Computer Vision - ECCV 2014 - 13th European Conference, Zurich, Switzerland, September 6-12, 2014, Proceedings, Part V*, volume 8693 of *Lecture Notes in Computer Science*, pages 740–755. Springer, 2014. doi: 10.1007/978-3-319-10602-1_48. URL `https://doi.org/10.1007/978-3-319-10602-1_48`.

Haotian Liu, Chunyuan Li, Qingyang Wu, and Yong Jae Lee. Visual instruction tuning. In Alice Oh, Tristan Naumann, Amir Globerson, Kate Saenko, Moritz Hardt, and Sergey Levine, editors, *Advances in Neural Information Processing Systems 36: Annual Conference on Neural Information Processing Systems 2023, NeurIPS 2023, New Orleans, LA, USA, December 10 - 16, 2023*, 2023. URL `http://papers.nips.cc/paper_files/paper/2023/hash/6dcf277ea32ce3288914faf369fe6de0-Abstract-Conference.html`.

Haotian Liu, Chunyuan Li, Yuheng Li, Bo Li, Yuanhan Zhang, Sheng Shen, and Yong Jae Lee. Llava-next: Improved reasoning, ocr, and world knowledge, January 2024. URL `https://llava-vl.github.io/blog/2024-01-30-llava-next/`.

Ilya Loshchilov and Frank Hutter. Decoupled weight decay regularization. *arXiv preprint arXiv:1711.05101*, 2017.

Holy Lovenia, Wenliang Dai, Samuel Cahyawijaya, Ziwei Ji, and Pascale Fung. Negative object presence evaluation (nope) to measure object hallucination in vision-language models. *arXiv preprint arXiv:2310.05338*, 2023.

Run Luo, Yunshui Li, Longze Chen, Wanwei He, Ting-En Lin, Ziqiang Liu, Lei Zhang, Zikai Song, Xiaobo Xia, Tongliang Liu, et al. Deem: Diffusion models serve as the eyes of large language models for image perception. *arXiv preprint arXiv:2405.15232*, 2024.

Meta. Llama-3.2-11b-vision-instruct, 2024. URL `https://huggingface.co/meta-llama/Llama-3.2-11B-Vision-Instruct`. Accessed: 2025-01-14.

Matthias Minderer, Alexey Gritsenko, and Neil Houlsby. Scaling open-vocabulary object detection, 2024. URL `https://arxiv.org/abs/2306.09683`.

Hossein Mirzaei, Mohammad Jafari, Hamid Reza Dehbashi, Ali Ansari, Sepehr Ghobadi, Masoud Hadi, Arshia Soltani Moakhar, Mohammad Azizmalayeri, Mahdieh Soleymani Baghshah, and Mohammad Hossein Rohban. Rodeo: Robust outlier detection via exposing adaptive out-of-distribution samples. *arXiv preprint arXiv:2501.16971*, 2025.

Arshia Soltani Moakhar, Eugenia Iofinova, Elias Frantar, and Dan Alistarh. Spade: Sparsity-guided debugging for deep neural networks, 2024. URL `https://arxiv.org/abs/2310.04519`.

Fahimeh Hosseini Noohdani, Parsa Hosseini, Aryan Yazdan Parast, Hamidreza Yaghoubi Araghi, and Mahdieh Soleymani Baghshah. Decompose-and-compose: A compositional approach to mitigating spurious correlation. In *Proceedings of the IEEE/CVF Conference on Computer Vision and Pattern Recognition*, pages 27662–27671, 2024.

OpenAI. Gpt-4 technical report, 2024. URL `https://arxiv.org/abs/2303.08774`.

Aryan Yazdan Parast, Basim Azam, and Naveed Akhtar. Ddb: Diffusion driven balancing to address spurious correlations, 2025. URL `https://arxiv.org/abs/2503.17226`.

Alec Radford, Jong Wook Kim, Chris Hallacy, Aditya Ramesh, Gabriel Goh, Sandhini Agarwal, Girish Sastry, Amanda Askell, Pamela Mishkin, Jack Clark, Gretchen Krueger, and Ilya Sutskever. Learning transferable visual models from natural language supervision, 2021a. URL `https://arxiv.org/abs/2103.00020`.

Alec Radford, Jong Wook Kim, Chris Hallacy, Aditya Ramesh, Gabriel Goh, Sandhini Agarwal, Girish Sastry, Amanda Askell, Pamela Mishkin, Jack Clark, et al. Learning transferable visual models from natural language supervision. In *International conference on machine learning*, pages 8748–8763. PMLR, 2021b.

Robin Rombach, Andreas Blattmann, Dominik Lorenz, Patrick Esser, and Björn Ommer. High-resolution image synthesis with latent diffusion models. In *Proceedings of the IEEE/CVF Conference on Computer Vision and Pattern Recognition (CVPR)*, pages 10684–10695, June 2022.

Shiori Sagawa, Pang Wei Koh, Tatsunori B Hashimoto, and Percy Liang. Distributionally robust neural networks for group shifts: On the importance of regularization for worst-case generalization. *arXiv preprint arXiv:1911.08731*, 2019.

Jascha Sohl-Dickstein, Eric A. Weiss, Niru Maheswaranathan, and Surya Ganguli. Deep unsupervised learning using nonequilibrium thermodynamics, 2015. URL https://arxiv.org/abs/1503.03585.

V Team, Wenyi Hong, Wenmeng Yu, Xiaotao Gu, Guo Wang, Guobing Gan, Haomiao Tang, Jiale Cheng, Ji Qi, Junhui Ji, Lihang Pan, Shuaiqi Duan, Weihan Wang, Yan Wang, Yean Cheng, Zehai He, Zhe Su, Zhen Yang, Ziyang Pan, Aohan Zeng, Baoxu Wang, Bin Chen, Boyan Shi, Changyu Pang, Chenhui Zhang, Da Yin, Fan Yang, Guoqing Chen, Jiazheng Xu, Jiale Zhu, Jiali Chen, Jing Chen, Jinhao Chen, Jinghao Lin, Jinjiang Wang, Junjie Chen, Leqi Lei, Letian Gong, Leyi Pan, Mingdao Liu, Mingde Xu, Mingzhi Zhang, Qinkai Zheng, Sheng Yang, Shi Zhong, Shiyu Huang, Shuyuan Zhao, Siyan Xue, Shangqin Tu, Shengbiao Meng, Tianshu Zhang, Tianwei Luo, Tianxiang Hao, Tianyu Tong, Wenkai Li, Wei Jia, Xiao Liu, Xiaohan Zhang, Xin Lyu, Xinyue Fan, Xuancheng Huang, Yanling Wang, Yadong Xue, Yanfeng Wang, Yanzi Wang, Yifan An, Yifan Du, Yiming Shi, Yiheng Huang, Yilin Niu, Yuan Wang, Yuanchang Yue, Yuchen Li, Yutao Zhang, Yuting Wang, Yu Wang, Yuxuan Zhang, Zhao Xue, Zhenyu Hou, Zhengxiao Du, Zihan Wang, Peng Zhang, Debing Liu, Bin Xu, Juanzi Li, Minlie Huang, Yuxiao Dong, and Jie Tang. Glm-4.5v and glm-4.1v-thinking: Towards versatile multimodal reasoning with scalable reinforcement learning, 2025. URL https://arxiv.org/abs/2507.01006.

Shengbang Tong, Erik Jones, and Jacob Steinhardt. Mass-producing failures of multimodal systems with language models. *Advances in Neural Information Processing Systems*, 36, 2024a.

Shengbang Tong, Zhuang Liu, Yuexiang Zhai, Yi Ma, Yann LeCun, and Saining Xie. Eyes wide shut? exploring the visual shortcomings of multimodal llms. In *Proceedings of the IEEE/CVF Conference on Computer Vision and Pattern Recognition*, pages 9568–9578, 2024b.

Maya Varma, Jean-Benoit Delbrouck, Zhihong Chen, Akshay Chaudhari, and Curtis Langlotz. Ravl: Discovering and mitigating spurious correlations in fine-tuned vision-language models. *arXiv preprint arXiv:2411.04097*, 2024.

Junyang Wang, Yuhang Wang, Guohai Xu, Jing Zhang, Yukai Gu, Haitao Jia, Ming Yan, Ji Zhang, and Jitao Sang. An llm-free multi-dimensional benchmark for mllms hallucination evaluation. *CoRR*, 2023.

Qizhou Wang, Yong Lin, Yongqiang Chen, Ludwig Schmidt, Bo Han, and Tong Zhang. Do CLIP models always generalize better than imagenet models? In *The Thirty-eighth Annual Conference on Neural Information Processing Systems*, 2024a. URL https://openreview.net/forum?id=wWyumwEYV8.

Zhecan Wang, Garrett Bingham, Adams Wei Yu, Quoc V Le, Thang Luong, and Golnaz Ghiasi. Haloquest: A visual hallucination dataset for advancing multimodal reasoning. In *European Conference on Computer Vision*, pages 288–304. Springer, 2024b.

Xiyang Wu, Tianrui Guan, Dianqi Li, Shuaiyi Huang, Xiaoyu Liu, Xijun Wang, Ruiqi Xian, Abhinav Shrivastava, Furong Huang, Jordan Lee Boyd-Graber, et al. Autohallusion: Automatic generation of hallucination benchmarks for vision-language models. *arXiv preprint arXiv:2406.10900*, 2024.

Yuanchen Wu, Lu Zhang, Hang Yao, Junlong Du, Ke Yan, Shouhong Ding, Yunsheng Wu, and Xiaoqiang Li. Antidote: A unified framework for mitigating lvlm hallucinations in counterfactual presupposition and object perception. In *Proceedings of the Computer Vision and Pattern Recognition Conference*, pages 14646–14656, 2025.

Wenqian Ye, Guangtao Zheng, Yunsheng Ma, Xu Cao, Bolin Lai, James M Rehg, and Aidong Zhang. Mm-spubench: Towards better understanding of spurious biases in multimodal llms. *arXiv preprint arXiv:2406.17126*, 2024.

Chenshuang Zhang, Fei Pan, Junmo Kim, In So Kweon, and Chengzhi Mao. Imagenet-d: Benchmarking neural network robustness on diffusion synthetic object. In *Proceedings of the IEEE/CVF Conference on Computer Vision and Pattern Recognition*, pages 21752–21762, 2024.

Jiaming Zhang, Junhong Ye, Xingjun Ma, Yige Li, Yunfan Yang, Chen Yunhao, Jitao Sang, and Dit-Yan Yeung. Anyattack: Towards large-scale self-supervised adversarial attacks on vision-language models. In *Proceedings of the IEEE/CVF Conference on Computer Vision and Pattern Recognition*, 2025a.

Jusheng Zhang, Kaitong Cai, Yijia Fan, Jian Wang, and Keze Wang. Cf-vlm: Counterfactual vision-language fine-tuning. *arXiv preprint arXiv:2506.17267*, 2025b.

Tianyi Zhang*, Varsha Kishore*, Felix Wu*, Kilian Q. Weinberger, and Yoav Artzi. Bertscore: Evaluating text generation with bert. In *International Conference on Learning Representations*, 2020. URL `https://openreview.net/forum?id=SkeHuCVFDr`.

Yunqing Zhao, Tianyu Pang, Chao Du, Xiao Yang, Chongxuan Li, Ngai-Man Cheung, and Min Lin. On evaluating adversarial robustness of large vision-language models. In *Thirty-seventh Conference on Neural Information Processing Systems*, 2023.

Guangtao Zheng, Wenqian Ye, and Aidong Zhang. Benchmarking spurious bias in few-shot image classifiers. In *European Conference on Computer Vision*, pages 346–364. Springer, 2024.

A Human Evaluation

To evaluate whether GHOST-generated images preserve the absence of the target object from a human perspective, we design a simple interface and collect annotations from peers. For both LLaVA and Qwen2.5-VL, we randomly sample 50 successful GHOST images per object across 10 object categories. To validate annotator reliability, we include control images that are known to contain the target object. These control images are generated using the same Diffusion unCLIP model, but conditioned on positive samples, ensuring the object is clearly present. Examples are shown in Figure 18. We include 50 control images per object.

Each annotator is shown a set of approximately 100 randomly selected images (comprising 20% control images, 40% GHOST–Qwen, and 40% GHOST–LLaVA) and asked "Is there a [target object] in this image?" with binary response options: "Yes" or "No." Before beginning the evaluation, annotators completed a brief training phase (Figure 10) that displayed a few labeled examples to calibrate their expectations.

In total, we collect 1,590 votes on LLaVA images, 1,607 on Qwen images, and 1,056 on control images, from 40 unique participants. Aggregate results are shown in Table 5, reporting the percentage of "Yes" responses in each group. Figure 11 further breaks down the human yes-rate by object class. We used the human evaluation setup from Moakhar et al. [2024].

Table 5: Human yes rate on control and GHOST-generated images.

Set of Images:	**Control Images**	**GHOST–LLaVA**	**GHOST–Qwen**
Human Yes Rate	91.2%	11.0%	13.7%

B DASH

We reproduce DASH results with Qwen2.5 and LLaVA. For LLaVA, we only evaluate DASH-LLM, a variant of DASH that relies solely on language model feedback. We omit DASH-OPT as it is too memory-intensive, even a batch size of 1 exceeds the limits of 80GB GPUs. For Qwen2.5, we evaluate both DASH-LLM and DASH-OPT. In DASH-OPT, we tune three parameters: step size, gradient clipping, and the VLM loss weight. In DASH-OPT, we tune three parameters: step size, gradient clipping, and the VLM loss weight. Specifically, we search step size and gradient clip values in $[0.1, 0.2, 0.4, 0.8]$, and the VLM loss weight in $[1, 2, 4, 6, 8]$. As our evaluation metric, we count the number of images that do not contain the target object according to an object detector but still mislead the MLLM into hallucinating its presence. We are unable to use ReLION-5B, as its KNN search service is private. Additionally, computing CLIP embeddings over the full dataset is computationally infeasible for us. Instead, we use the COCO dataset for our experiments. The corresponding results are shown below.

In the test you will be shown an image and a prompt like:

Label the Image

Is there a **Bird** in this image?

No, it doesn't   Yes, it exists

The key rule is:

> Only answer "Yes" if you can clearly see the target object itself — not just its usual surroundings.

In other words:
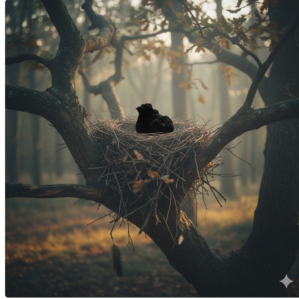
- If the background looks like the place where the object is often found, but the object itself is not visible, answer No, it doesn't .
- If the object is visible, even in an unusual or surprising setting, answer Yes, it exists .
- *Example:* A dark, round shape on a tree branch should be labeled No, it doesn't if the target object is *bird* (because you can't actually see a bird).
- *Example:* A camel standing in the middle of a living room should be labeled Yes, it exists if the target object is *camel* (because the camel itself is visible).

Next: Practice Test »

Step 1

Label the Image

Is there a **Bird** in this image?

Yes, it exists   No, it doesn't

Step 2

Label the Image

Is there a **Camel** in this image?
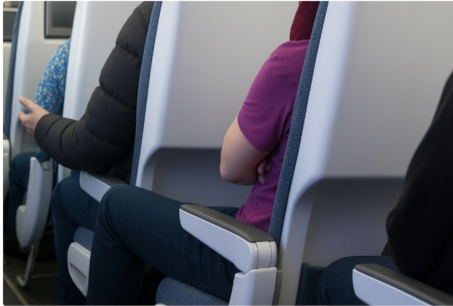
Yes, it exists   No, it doesn't

Step 3

Label the Image

Is there an **Airplane** in this image?

Yes, it exists   No, it doesn't

Step 4

Figure 10: Human Evaluation Training Phase
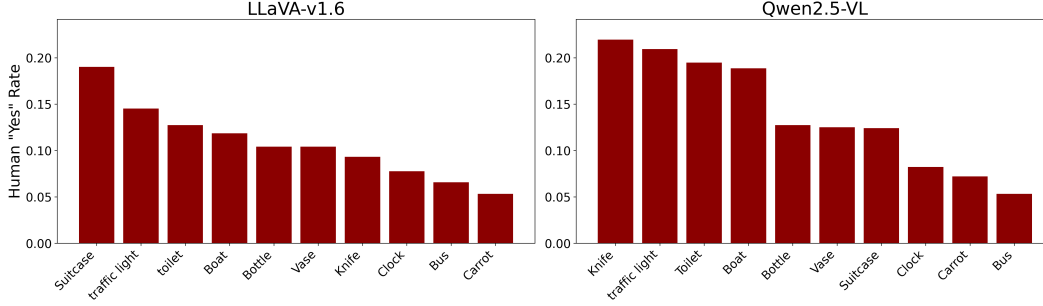
Figure 11: Human Yes-Rate by object class

Table 6: The number of successful image found by DASH on COCO

Method	Number of Found Images
DASH-opt (qwen2.5)	42
DASH-LLM (qwen2.5)	57
DASH-LLM (llava)	153

C Mapper

C.1 Mapper Training

To bridge the embedding spaces, we introduce a mapper Π that projects the CLS token from the CLIP vision encoder space $\mathcal{V}_{\text{CLIP}}$ into the vision encoder space of the target multimodal model. We design a simple multi-layer perceptron (MLP) to achieve this mapping. Specifically, the mapper takes the CLIP CLS token $\mathbf{z}_{\text{CLIP}} \in \mathbb{R}^{d_{\text{CLIP}}}$ as input and outputs a sequence of N tokens, each of dimension $d_{\mathcal{M}}$, suitable for the target model:

$$\Pi : \mathbb{R}^{d_{\text{CLIP}}} \; \to \; \mathbb{R}^{N \times d_{\mathcal{M}}}.$$

Concretely, we first broadcast the CLS token across N positions, obtaining

$$\mathbf{Z}_{\text{rep}} = [\mathbf{z}_{\text{CLIP}}, \ldots, \mathbf{z}_{\text{CLIP}}] \in \mathbb{R}^{N \times d_{\text{CLIP}}}.$$

In parallel, we maintain a set of learnable context tokens

$$\mathbf{E} = \{\mathbf{e}_1, \ldots, \mathbf{e}_N\}, \quad \mathbf{e}_i \in \mathbb{R}^{d_{\mathcal{M}}},$$

which provide token-specific priors for the mapping. For each position i, we concatenate the repeated CLS token with its corresponding learnable context token:

$$\mathbf{h}_i = [\mathbf{z}_{\text{CLIP}}; \mathbf{e}_i] \in \mathbb{R}^{d_{\text{CLIP}} + d_{\mathcal{M}}}.$$

Table 7: Number of successful image found by DASH on COCO by class name

Class/Method	DASH-opt (qwen2.5)	DASH-LLM (qwen2.5)	DASH-LLM (llava)
traffic light	0	0	0
carrot	1	0	10
knife	0	2	14
clock	13	11	7
toilet	0	0	0
boat	2	0	0
suitcase	3	1	11
bottle	20	42	80
vase	3	0	23
bus	0	1	8

Table 8: Successful images found by DASH on COCO by class name

Class/Method	DASH-opt (qwen2.5)	DASH-LLM (qwen2.5)	DASH-LLM (llava)
clock			
suitcase			
bottle			

The sequence $\mathbf{H} = \{\mathbf{h}_1, \ldots, \mathbf{h}_N\}$ is then passed through an MLP with two hidden layers of size d_h, each followed by a GELU activation:

$$\mathbf{y}_i = \mathrm{MLP}(\mathbf{h}_i), \quad \mathbf{Y} = \{\mathbf{y}_1, \ldots, \mathbf{y}_N\} \in \mathbb{R}^{N \times d_{\mathcal{M}}}.$$

The learnable context embeddings $\mathbf{E}$ serve as token-specific conditioning vectors. Although the MLP parameters are shared across all positions, the concatenation $[\mathbf{z}_{\mathrm{CLIP}}; \mathbf{e}_i]$ ensures that each target token i is shaped by both the global CLIP semantics and its unique context embedding. For training the mapper, we used the AdamW optimizer with cosine annealing learning rate scheduling. The details of the training process and hyperparameters are summarized in Table 10.

C.2 Model Selection.

For model selection, we randomly sampled 100 images containing a given object class and 100 images without it from the COCO training set. We then evaluated the accuracy of the MLLM using the bridged embeddings obtained from the mapper Π, and the same prompts used in the main method (e.g. Do you see the object in the image). We considered six object classes: *vase*, *boat*, *bird*, *giraffe*, *car*. These classes were selected to cover a range of object characteristics: small objects such as *remote*, which require fine-grained detail to be detected from the mapper, and large objects such as *giraffe*, which are comparatively easier for the MLLM to recognize. In Table 9, we report the accuracy

Table 9: Ablation on hidden dimension and context dimension for the projector, evaluated on LLaVA and Qwen. Numbers report accuracy (%). The final configuration selected for our experiments is highlighted in **bold**.

	Hidden Dim	**512**	**1024**	**2048**	**4096**
LLaVA	Context = 6144	70.17	72.17	72.75	73.67
	Context = 4096	70.83	**72.25**	72.50	72.67
Qwen	Context = 6144	69.50	71.08	73.50	73.92
	Context = 4096	68.08	71.67	**73.92**	72.75

Table 10: Training hyperparameters for each model.

Model	LR	Epochs	Batch Size	Weight Decay	Scheduler	Warmup Steps
GLM	2e-4	10	32	0.01	Cosine ($T_{\max} = 10$)	1000
LLaVA	2e-4	10	64	0.01	Cosine ($T_{\max} = 10$)	1000
Qwen	2e-4	10	32	0.01	Cosine ($T_{\max} = 10$)	1000

obtained with different settings of context dimension and hidden dimension. The final configuration selected for our experiments is highlighted in **bold**. We chose this setting by balancing accuracy with model size and efficiency, ensuring that the mapper achieves strong performance without incurring unnecessary computational cost.

C.3 Mapper Evaluation

Inspired by [Liu et al., 2023], we assess the reconstruction capability of the MLP connector f using GPT-4 as a judge. For each input image x, we first obtain the response of the target MLLM (e.g., LLaVA) when conditioned on the true image embedding $\mathcal{V}_{\mathcal{M}}$. We then provide this response, together with the ground-truth COCO object annotations, to GPT-4, which rates the consistency between the response and the annotations. Next, we replace the image input with the projected embedding $\Pi(\mathcal{V}_{\text{clip}}(x))$, obtain the MLLM response, and request GPT-4 to rate it in the same way. The relative score between the two ratings serves as a measure of the mapper's ability to reconstruct the semantics of the image. We define the relative score as the ratio between the GPT rating of the projected-embedding response and that of the real-image response which quantifies how much semantic information from the original image embedding is retained after projection. Further details on this experiment and the evaluation prompt are provided in the appendix. For this study, we randomly selected 100 images from the COCO dataset. The results on LLaVA-v1.6, Qwen2.5-VL, and GLM are reported in Table 11. As shown, the projector preserves most of the semantic content of the original image while substantially reducing computational cost.

D Latent Diffusion Models

Diffusion probabilistic models [Sohl-Dickstein et al., 2015, Ho et al., 2020] generate samples that approximate the data distribution through a parameterized Markov chain. The core idea is to gradually corrupt a clean sample with Gaussian noise (forward process), and then learn to reverse this process (backward process) to recover clean data.

Latent Diffusion Models (LDMs) [Rombach et al., 2022] perform this procedure in a compressed latent space. Let z_0 denote the latent representation of a clean image obtained via a VAE encoder ($\mathcal{E}_{vae}$.) The forward noising process defines a distribution

$$q(z_t \mid z_0) = \mathcal{N}\big(z_t;\ \sqrt{\bar{\alpha}_t}\, z_0,\ (1 - \bar{\alpha}_t)I\big),$$

where $t \in \{1, \ldots, T\}$ is the diffusion timestep, α_t are variance schedule parameters, and $\bar{\alpha}_t = \prod_{s=1}^{t} \alpha_s$. Thus, a latent z_t can be obtained directly by applying the scheduler to z_0, progressively injecting noise as t increases.

Table 11: Evaluation of Mapper using GPT-4 as judge. Scores are reported for MLLM responses conditioned on the real image and on the reconstructed embedding.

Source Model	Input Type	Basic Score	Relative Score
Qwen2.5-VL	Real Images	89.6	76.0
	Reconstructed	68.1	
LLaVA-v1.6	Real Images	84.9	54.5
	Reconstructed	46.3	
GLM4.1-Thinking	Real Images	94.0	75.6
	Reconstructed	71.1	

Table 12: Class-wise results with success rate and number of successful samples in $t = 15$ noise level setting.

Class	Images Optimized	Success Rate	Successful Samples
Vase	198	0.32	63
Knife	198	0.46	91
Boat	200	0.24	48
Bottle	188	0.57	107
Total / Mean	784	0.40	309

The reverse process learns to iteratively denoise, starting from $z_T \sim \mathcal{N}(0, I)$ or, more generally, from a noisy latent z_t:

$$z_{t-1} = \frac{1}{\sqrt{\alpha_t}} \left(z_t - \frac{1 - \alpha_t}{\sqrt{1 - \bar{\alpha}_t}} \, \epsilon_\theta(z_t, t, C) \right) + \sigma_t \, \mathbf{z},$$

where ϵ_θ is a UNet denoiser trained on large-scale data, C is an optional conditioning signal (e.g., text or image embeddings), and $\mathbf{z} \sim \mathcal{N}(0, I)$. Finally, the clean latent z_0 is decoded through the VAE decoder $\mathcal{D}$ to obtain the generated sample in pixel space.

In this work, we employ the Stable Diffusion unCLIP model [Rombach et al., 2022], which conditions the denoising process on CLIP image embeddings [Radford et al., 2021a]. Given an image x and a CLIP image encoder $\mathcal{E}_{\text{clip}}$, the model generates a new sample conditioned on $\mathcal{E}_{\text{clip}}(x)$, ensuring that the output preserves the high-level semantics of x.

E GHOST Optimization

E.1 GHOST Without CLIP Sorting

For evaluating the performance of GHOST without CLIP-based sorting, we conduct an experiment on four classes: "Boat", "Vase", "Knife", and "Bottle". For each class, we randomly select 200 samples that do not have the target object from their categories based on COCO annotations. When we select the pictures without sorting, the initial images are farther from the target object semantically, so more changes are needed to induce hallucination. To overcome this issue, we use noise level $t = 15$ (in contrast to our standard setting where the noise level is $t = 30$) as a hyperparameter to add more noise to the image and be able to change the image further. We also select $\tau = 0.6$ to soften the constraint of optimization; all the other hyperparameters are the same as the standard setting. As reported in Table 12, the success rate is comparable to our method in the sorting setting. Qualitative samples with $t = 15$ as the noise level are also shown in Figure 12. As shown in Figure 12, when the noise level is decreased, more changes are applied to the initial images to induce hallucination.

E.2 Text representation

The $\mathcal{L}_{\text{clip}}$ term in our objective function (Equation 4) prevents the optimized image embedding z from directly encoding the semantics of the target object. To make this regularization robust, we use an enhanced, compositional text representation of the target object, rather than a single word
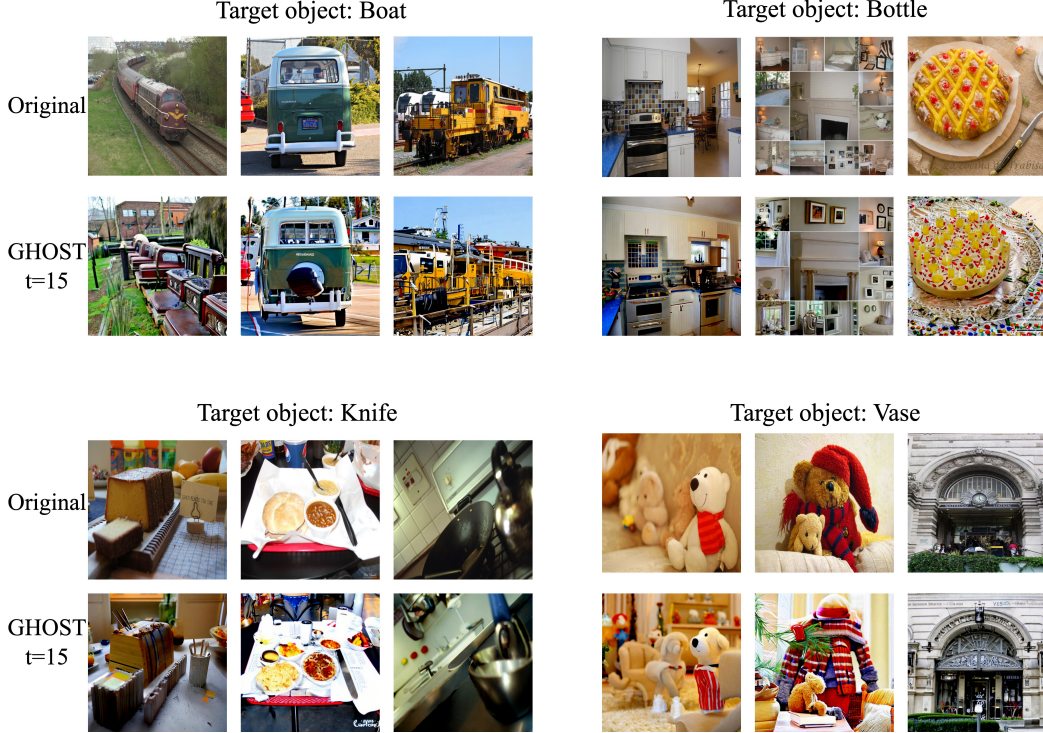
Figure 12: Qualitative samples from GHOST on Qwen2.5 VL 7B, with noise level $t = 15$. The top row shows the original images, and the bottom row shows samples generated with GHOST.

textual description. This representation helps push the optimized image embedding away from a comprehensive semantic understanding of the object, encouraging the MLLM to hallucinate based on subtle visual cues instead of object generation.

Our compositional text representation for a target object t is constructed from three distinct sources, whose CLIP embeddings are then combined via a weighted average:

1. **Direct Object Description:** We start with a straightforward descriptive sentence, such as "A photo of a *class_name*". This provides a simple, unambiguous representation of the object. Let its CLIP embedding be E_D.

2. **Generic Contextual Templates:** We utilize a set of generic templates to capture various linguistic contexts. These templates are universal across all target objects and are listed in Listing 1. For a given target object t, these templates are filled to form specific phrases (e.g., "A scene featuring a vase"). Up to $N_{GT} = 4$ such template-based phrases are selected, and their CLIP embeddings are denoted as $E_{GT,j}$ for $j = 1, \ldots, N_{GT}$.

3. **Mined COCO Captions:** We augment the representation by identifying and embedding actual captions from the COCO training dataset that explicitly contain the target object. Incorporating real-world descriptive language captures nuanced ways humans refer to objects in visual contexts. Up to $N_{CC} = 5$ such mined captions are selected, and their CLIP embeddings are denoted as $E_{CC,k}$ for $k = 1, \ldots, N_{CC}$.

These CLIP text embeddings are combined into a single 'compositional embedding' (E_{comp}) using a weighted average. The formula is:

$$E_{\text{comp}} = w_D E_D + \sum_{j=1}^{N_{GT}} \frac{w_{GT}}{N_{GT}} E_{GT,j} + \sum_{k=1}^{N_{CC}} \frac{w_{CC}}{N_{CC}} E_{CC,k} \qquad (7)$$

where $w_D = 0.3$, $w_{GT} = 0.4$, and $w_{CC} = 0.3$ are the base weights for the direct description, generic templates, and COCO captions, respectively. The weights for generic templates and COCO

Table 13: Attack hyperparameters for each victim model.

Model	lr	total steps	τ.	N	Guidance Scale	λ_{clip}	λ_{reg}	OD thr.	t	num_inf.
Qwen	0.1	100	0.8	4	5.0	15.0	10.0	0.5	30	50
LLaVA	0.1	100	0.8	4	5.0	15.0	10.0	0.5	30	50
GLM	0.2	125	0.5	5	5.0	0.5	1.5	0.5	30	50

Table 14: Model identifiers.

Model	ID / Name
Qwen	Qwen/Qwen2.5-VL-7B-Instruct
LLaVA	llava-hf/llava-v1.6-mistral-7b-hf
GLM	THUDM/GLM-4.1V-9B-Thinking

captions are distributed evenly among their respective constituent embeddings. This robust E_{comp} is then used as the specific text query $\mathbf{T}_q$ for the $\mathcal{L}_{\text{clip}}$ loss term, defined as $\cos(z, \mathcal{V}_{\text{CLIP}}(E_{\text{comp}}))$. By minimizing this loss, we encourage z to be *dissimilar* to E_{comp}, thereby preventing the optimized image embedding from inadvertently encoding the actual presence of the target object.

E.3 Hyperparameters

We summarize the attack hyperparameters for each victim model in Table 13, while the corresponding model identifiers are listed separately in Table 14. We tuned the hyperparameters based on our evaluation metrics, including image quality (FID score), attack success rate, and human evaluation, which all are discussed in the main paper.

E.4 Prompts

At each step of the optimization, we randomly select a prompt from our template set to avoid overfitting to a specific prompt. The prompts are designed to query the presence of the target object in a binary (Yes/No) format. This randomization ensures that the optimization does not exploit superficial linguistic patterns but instead focuses on inducing the desired hallucination. The complete set of prompt templates is provided in Listing 2.

E.5 Effect of λ_{reg}

To assess the effect of λ_{reg}, we apply GHOST to the GLM4.1 Thinking model with $\lambda_{reg} \in \{1.0, 1.5, 2.0\}$. Since the FID score is sensitive to the number of samples, for each pair of λ_{reg} values we select only the samples that are successful in both settings, and then compute the FID score against both the COCO validation set and the original images. As reported in Table 15, increasing λ_{reg} consistently makes the generated images more similar to the original ones, leading to improved realism, as reflected by lower FID scores.

E.6 Effect of λ_{clip}

Increasing λ_{clip} encourages semantic separation between the guiding embedding z and the target-object semantics. We implement GHOST on two target objects ("traffic light" and "Boat", 200 images each) on Qwen2.5-VL with $\lambda_{\text{clip}} \in \{5, 10, 15, 20\}$ and $N=4$ samples per image to evaluate the effect of it. As shown in Fig. 13, larger λ_{clip} consistently reduces the count of OD-filtered samples, indicating that the regularization term achieves its intended effect by suppressing target-object semantics in the generated images. From $\lambda_{\text{clip}} = 5$ to 15, stronger suppression of target-object cues makes it harder for the MLLM to answer "yes", so more samples are generated and also a larger share of generated samples fail to trigger hallucination. At $\lambda_{\text{clip}} = 20$, this term becomes over-weighted: fewer runs satisfy $p(y^* \mid \mathbf{X}_q, \Pi(z)) \geq \tau_{\text{yes}}$, and more runs hit the maximum (100) steps of optimization (e.g., $10 \rightarrow 20$)

Table 15: Ablation study on λ_{reg}. FID scores computed on the intersected set of generated images, with respect to the original images and the COCO validation set. The lower FID in each pair is shown in bold.

Gen. Data	λ_{reg}	Orig	Val
(1.0, 1.5)	1.0	127.46	145.05
	1.5	**125.11**	**144.11**
(1.0, 2.0)	1.0	148.85	169.74
	2.0	**138.67**	**163.84**
(1.5, 2.0)	1.5	144.25	168.20
	2.0	**135.79**	**163.54**

Table 16: Sample statistics for different objects with Qwen2.5 as the victim model.

Object	Samples Considered	Image Generated	Image Filtered	Successful Samples
Boat	915	3141	191	258
Bottle	881	2746	21	383
Bus	891	2995	311	244
Carrot	956	3353	132	228
Clock	962	3473	392	175
Knife	966	2368	114	353
Suitcase	949	3067	234	367
Toilet	969	3368	817	289
Traffic light	992	3291	424	312
Vase	942	3279	101	207

E.7   Effect of τ

We implement GHOST with two target objects (200 images each) on LLaVA-1.6, varying $\tau \in \{0.5, 0.6, 0.7, 0.8, 0.9\}$ and using $N{=}4$ generations per image. As shown in Fig. 14, increasing τ tightens the optimization constraints, and the number of generated samples consistently decreases. At lower τ, the embedding contains weaker target-object cues, so more generations fail to elicit a "yes" from the MLLM. For $\tau \in \{0.5, 0.6, 0.7\}$, the ratio of total to unsuccessful generations is similar, and the number of successful samples is nearly unchanged.

F   GHOST Additional Results

In this section, we provide extended qualitative and quantitative results to complement the main paper. Figures 15, 16, and 17 present qualitative examples of GHOST applied to Qwen2.5, LLava-1.6, and GLM-4.1Thinking, respectively, showing the original images alongside GHOST-generated samples and the corresponding model responses. Tables 16, 17, and 18 report detailed sample statistics for each object category across the three victim models, including the number of generated, filtered, and successful samples. Finally, Tables 19, 20, and 21 provide class-wise transferability results, highlighting how GHOST-induced hallucinations on one victim model transfer to others.

G   Finetuning

A growing body of work has shown that models robustness can be substantially improved through fine-tuning on synthetically generated or edited images [Augustin et al., 2025, Parast et al., 2025, Wang et al., 2024b, Wu et al., 2025, Azizmalayeri et al., 2022, Zhang et al., 2025b, Mirzaei et al., 2025, Bai et al., 2025b].

Table 17: Sample statistics for different objects with LLlava-1.6 as the victim model.

Object	Samples Considered	Image Generated	Image Filtered	Successful Samples
Boat	863	2804	63	270
Bottle	763	1558	4	221
Bus	786	2221	168	178
Carrot	948	3041	101	218
Clock	927	2588	198	298
Knife	843	1092	29	188
Suitcase	885	1644	100	364
Toilet	945	3081	543	268
Traffic light	967	2508	160	241
Vase	859	1499	33	216

Table 18: Sample statistics for different objects with GLM-4.1 Thinking as the victim model.

Object	Samples Considered	Image Generated	Image Filtered	Successful Samples
Boat	847	2032	202	305
Bottle	710	1346	53	348
Bus	764	2102	373	321
Carrot	939	3130	76	272
Clock	937	3146	297	290
Knife	968	2644	80	271
Suitcase	937	2322	276	328
Toilet	942	1932	486	217
Traffic light	979	2294	192	176
Vase	866	2137	141	286

G.1 Fine-tuning protocol.

We fine-tune Qwen2.5VL-7B using images generated by our GHOST procedure (targeting Qwen2.5VL -7B) to assess whether such counterfactual samples improve model performance. We include this as a proof-of-concept demonstration, with scaling to larger datasets and all classes reserved for future work. We adopt LoRA [Hu et al., 2022] for parameter-efficient adaptation; the exact hyperparameters are listed in Table 22.

G.2 Dataset construction.

We constructed a balanced fine-tuning set by pairing each *negative* sample (a GHOST-generated image) with one *positive* sample. Positives were synthesized with Stable Diffusion unCLI P(SD unCLIP) [Rombach et al., 2022], with images which contain the object as input. We intentionally avoided using real COCO images as positives to prevent shortcut learning (i.e., the degenerate rule "synthetic→negative, real→positive").

To increase label fidelity for the synthesized positives, we relied on the COCO annotations , and filtered candidate generations by ranking their CLIP embeddings against a compositional text embedding of the target object (Sec. E.2), keeping the highest-scoring images to give inputs to SD unCLIP model. This process improves the likelihood that the positive set truly depicts the intended object while keeping the data domain consistent (synthetic vs. synthetic) across classes. Examples of positive samples generated are shown in Figure 18.

G.3 Model selection

We use POPE on the COCO training split as our checkpointing criterion. After each epoch, we compute the POPE *Random* setting on 1,000 samples and retain the checkpoint with the highest F1 score.

Table 19: Class-wise transferability with Qwen2.5 as the victim model.

Object	LLaMA	LLava-1.6	GLM
Boat	67.8	68.2	79.7
Bottle	67.1	66.1	85.4
Bus	73.0	49.6	85.4
Carrot	52.2	48.3	64.7
Clock	57.7	70.3	75.6
Knife	64.0	64.9	52.7
Suitcase	69.2	70.3	58.7
Toilet	73.4	52.9	73.5
Traffic light	67.7	64.4	78.1
Vase	58.9	61.8	71.7

Table 20: Class-wise transferability with Llava-1.6 as the victim model.

Object	LLaMA	Qwen2.5	GLM
Boat	51.9	56.7	51.9
Bottle	50.2	55.2	63.2
Bus	48.9	47.2	49.0
Carrot	47.3	57.3	57.6
Clock	41.3	52.0	53.3
Knife	52.1	52.1	37.4
Suitcase	50.6	47.0	32.0
Toilet	60.1	55.2	54.7
Traffic light	47.7	51.0	57.1
Vase	46.8	53.7	56.5

Table 21: Class-wise transferability results with GLM-4.1Thinking as the victim model.

Object	LLaMA3.2	Qwen2.5	LLava1.6
Boat	75.7	67.0	66.0
Bottle	75.6	72.5	62.8
Bus	62.6	42.7	35.8
Carrot	45.2	52.2	31.6
Clock	56.1	56.1	65.9
Knife	84.5	69.0	68.6
Suitcase	82.2	70.9	68.1
Toilet	69.4	68.9	48.4
Traffic light	71.7	72.8	53.9
Vase	64.6	63.2	64.9

G.4 Model Evaluation

We evaluate the fine-tuned model on our generated images from other models (victim models) and on POPE using the COCO validation set. Specifically, we use the POPE *Adversarial*, *Random*, and *Popular* settings with maximum samples of $n = 3000$ samples. The results are available in the main paper. To evaluate how much fine-tuning impacted the overall performance of the MLLM, we evaluated the model on VQA and captioning tasks. For the VQA task, we leverage the small VQAv2 dataset from the Hugging Face implementation[2]. The dataset consists of an image–question pair and a single-word ground-truth answer. We compute accuracy for both the base model and the fine-tuned model on this task to assess the impact of fine-tuning. For the captioning task, we leverage COCO validation images and captions as ground truth. We generate captions for all COCO validation images with the base model and the fine-tuned model using the prompt: "Write a short caption for the given image." Then we compute BERTScore [Zhang* et al., 2020] using the generated captions and COCO annotations as ground truth.

---

[2]https://huggingface.co/datasets/merve/vqav2-small

Table 22: Fine-tuning hyperparameters and LoRA configuration.

LoRA configuration	
Rank (r)	8
Alpha	32
Dropout	0.05
Training setup	
Optimizer	Adam
Learning rate	5×10^{-6}
Epochs	15
Batch size	16
Warmup ratio	0.10
Scheduler	Cosine with warmup

```
generic_templates = [
    "A scene featuring a {class_name}",
    "An image showing a {class_name}",
    "A photograph with a {class_name}",
    "A picture containing a {class_name}"
]
```

Listing 1: Generic contextual templates used for constructing the enhanced text representation. The placeholder 'class_name' is replaced with the target object name during embedding generation.

```
templates = [
    "Do you see a {obj} in the image? Answer with 'Yes' or 'No'.",
    "Is there a {obj} here? Answer with 'Yes' or 'No'.",
    "Does the image contain a {obj}? Answer with 'Yes' or 'No'.",
    "Can you find a {obj} in this picture? Answer with 'No
    '.",
    "Would you say there's a {obj} here? Answer with 'Yes' or 'No'.",
    "Is a {obj} present in this image? Answer with 'Yes' or 'No'.",
]
```

Listing 2: Binary question templates used for querying the presence of the target object. The placeholder 'obj' is replaced with the object name (e.g., "boat", "vase") during optimization.
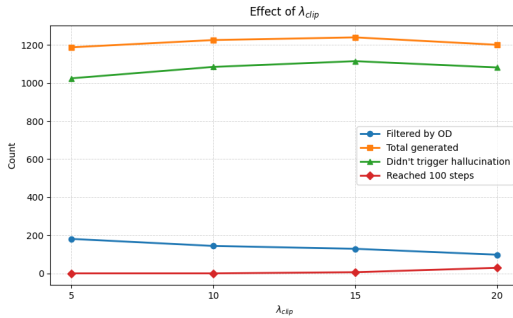

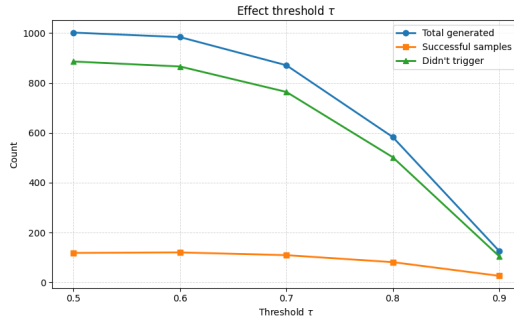Figure 13: The effect of λ_{clip}.

Figure 14: The effect of τ.

Is there a boat in this image? Answer with yes or no, then explain shortly.

: No, there is no boat in the image. The image shows a kitchen area with a stove, sink, and some kitchen utensils. There are no boats visible in this scene.

: Yes, the image shows the interior of a boat. The presence of a steering wheel, sink, and cabinetry are typical features found on a boat's deck or cabin.

Is there a clock in this image? Answer with yes or no, then explain shortly.

:No, there is no clock in the image. The structure appears to be a small tower or spire with a cross at the top and some architectural details, but there is no visible clock face or mechanism.

:Yes, there is a clock in the image. It is located on the right side of the structure and appears to be part of a decorative architectural element.

Is there a bus in this image? Answer with yes or no, then explain shortly.
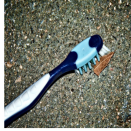

: No, there is no bus in the image. The image shows a cat lying on the floor next to some suitcases and a patterned bag. There are no vehicles, including buses, visible in the picture.

: Yes, there is a bus in the image. The interior of the vehicle shows seats and a patterned wall that is characteristic of a bus, along with a cat lying on the floor, which suggests it might be a pet-friendly bus or a converted bus into a living space.

Is there a knife in this image? Answer with yes or no, then explain shortly.

:No, there is no knife in the image. The object present is a toothbrush with a piece of paper stuck to it.

:Yes, there is a knife in the image. The object has a handle and a blade, which are characteristic features of a knife. The blade appears to be modified or decorated with an eye-like design, but it still retains the essential shape and structure of a knife.

Is there a traffic light in this image? Answer with yes or no, then explain shortly.

: No, there is no traffic light in the image. The image shows a fire hydrant painted to look like a person wearing a hat and a yellow jacket, with a car and a street in the background.

: Yes, there is a traffic light in the image. It appears to be a pedestrian crossing signal, which is used to control pedestrian traffic at intersections. The signal has a yellow housing and is mounted on a pole, indicating it's designed for pedestrians to cross safely when the light is green.

Is there a suitcase in this image? Answer with yes or no, then explain shortly.

:No, there is not a suitcase in the image. The object in question appears to be a pet carrier, which is used for transporting animals, as indicated by the presence of what looks like a small animal inside and the design of the container.

:Yes, there is a suitcase in the image. It appears to be a large, white, hard-shell suitcase with various items and decorations attached to it, including what looks like a small cage or container on top of it.

Is there a carrot in this image? Answer with yes or no, then explain shortly.

:No, there is no carrot in the image. The image shows a can of Campbell's tomato soup and a banana.

:Yes, there is a carrot in the image. The object on the right side of the image has the characteristic shape and color of a carrot, including its root end and leafy top.

Is there a toilet in this image? Answer with yes or no, then explain shortly.

:No, there is no toilet in the image. The image shows a row of sinks with soap dispensers and mirrors above them, which are typical features in a public restroom or bathroom setting.

:Yes, there is a toilet in the image. The image shows a public restroom with multiple urinals and a toilet visible on the left side of the frame.

Figure 15: Qualitative samples from GHOST on Qwen2.5 as the victim model, along with Qwen's responses to each image. For each pair, the top image shows the original input, while the bottom image shows the corresponding sample generated by GHOST.

Is there a boat in this image? Answer with yes or no, then explain shortly.
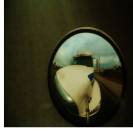
:No, there is no boat in this image. The image shows a truck reflected in a side mirror.
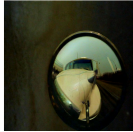
:Yes, there is a boat in this image. It is reflected in a mirror or a shiny surface.

Is there a clock in this image? Answer with yes or no, then explain shortly.

: No, there is no clock in this image. The image features a parking meter on the side of a street.

:Yes, there is a clock in this image. It is a parking meter with a clock on the front of it.

Is there a bus in this image? Answer with yes or no, then explain shortly.

: No, there is no bus in this image. The vehicle in the image is a Volkswagen van.

: Yes, there is a bus in this image. It is an old red Volkswagen bus.

Is there a knife in this image? Answer with yes or no, then explain shortly.

:No, there is no knife in this image. The image shows a toothbrush on a wooden surface.

:Yes, there is a knife in the image. It is lying on a wooden surface next to a toothbrush.

Is there a vase in this image? Answer with yes or no, then explain shortly.

:No, there is no vase in this image. The image shows a bowl of fruit and a glass of juice on a countertop.

: Yes, there is a vase in the image. It is located on the countertop, next to the bowl of oranges.

Is there a bottle in this image? Answer with yes or no, then explain shortly.

:No, there is no bottle in this image. The image features a vase with a red rose in it.

:Yes, there is a bottle in this image. It is a vase holding a flower.

Is there a carrot in this image? Answer with yes or no, then explain shortly.
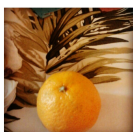
:No, there is no carrot in this image. The image features an orange.
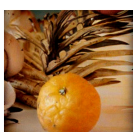
:Yes, there is a carrot in this image. It is located in the background, behind the orange.

Is there a toilet in this image? Answer with yes or no, then explain shortly.

:No, there is no toilet in this image. The image shows a sink and a small pink figurine on a shelf above the sink.

:Yes, there is a toilet in this image. It is a small, white toilet situated in a bathroom.

Figure 16: Qualitative samples from GHOST on LLava1.6 as the victim model, along with LLava's responses to each image. For each pair, the top image shows the original input, while the bottom image shows the corresponding sample generated by GHOST.

Target object: Vase

:Got it, let's look at the image. The object shown is an elephant-shaped figurine, not a vase. Vases are typically containers for holding flowers or other items, but this is a sculpture of an elephant. So the answer should be No.

:Got it, let's look at the image. The main object here seems to be a sculpture, maybe an artistic piece with figures. Wait, is there a vase? Wait, the sculpture might be a vase-shaped object? Wait, no, let me check again. Wait, the image shows a sculpture that might be a vase, but let's confirm. Wait, the question is if there's a vase. Let me check the details. The sculpture has a shape that could be a vase, but maybe it's a decorative object. Wait, the image has a sculpture that might be a vase. Wait, no, maybe not. Wait. ... so the answer is Yes.

Target object: Boat

:Got it, let's look at the image. The scene shows a bridge with a "STOP" sign, ropes, and a dock area. There's no boat visible in the image. So the answer should be No.

:Got it, let's look at the image. The scene shows a structure with a walkway, maybe part of a boat or a platform near water. The setting seems to be on a boat or a floating structure. So, is there a boat? Let's check. The area with the walkway and the water suggests it's part of a boat. So the answer would be Yes

Target object: Toilet

Got it, let's look at the image. The question is asking if there's a toilet. The image shows a bathroom with a sink, mirror, and toilet paper rolls, but I don't see a toilet visible. Wait, maybe the toilet is not in the frame? Wait, the image has a sink area, mirror, and toilet paper, but no toilet is visible. So the answer would be No.

:Got it, let's look at the image. There's a white toilet visible near the sink area. So the answer should be Yes.

Target object: Knife

:Got it, let's look at the image. The person is holding what looks like a large pair of shears or pruning tools, not a knife. Wait, the question is about a knife. Let me check again. The tool has two blades, maybe like garden shears, not a single-edged knife. So there's no knife visible. Therefore, the answer is No

:Got it, let's look at the image. The person is holding a large tool, which looks like a knife or a sword.Wait, the object has a blade, so it's a knife-like weapon. So the answer should be Yes

Target object: Carrot

:Got it, let's look at the picture. The question is asking if there's a carrot. Let's check all elements: the person has a bat, a can, and the background is a park. There's no carrot visible. So the answer is No.

: Got it, let's look at the image. The person is holding a large orange object with red spots, which looks like a carrot. Wait, is it a carrot? The object has the shape and color of a carrot, so I need to check. The question is whether there's a carrot. The object in the left hand is orange with red, maybe a carrot. So the answer would be Yes.

Target object: Suitcase

:Got it, let's look at the image. The container is a white fabric box, maybe a storage bin, not a suitcase. Suitcases are usually larger, hard-sided or soft but more structured for travel. This is a small storage box under a piece of furniture. So the answer should be No.

:Got it, let's look at the image. There's a beige bag with text, maybe a suitcase? Wait, the question is about a suitcase. The object behind the teddy bear looks like a suitcase or a bag. So is there a suitcase? Let's check. The image has a bag with "Glui" text, maybe a suitcase. So the answer would be Yes.

Figure 17: Qualitative samples from GHOST on GLM4.1Thinking as the victim model, along with GLM's thinking phase in each image. For each pair, the top image shows the original input, while the bottom image shows the corresponding sample generated by GHOST.

Vase	Bus	Knife	Boat

Traffic Light	Suticase	Carrot	Bottle

Figure 18: Positive samples generated with Stable Diffusion unCLIP [Rombach et al., 2022]